



1 Long-term NO_x measurements in the remote
2 marine tropical troposphere
3

4 Simone T. Andersen^{1*}, Lucy J. Carpenter¹, Beth S. Nelson¹, Luis Neves², Katie A. Read^{1,3},
5 Chris Reed⁴, Martyn Ward¹, Matthew J. Rowlinson^{1,3}, James D. Lee^{1,3}

6 ¹Wolfson Atmospheric Chemistry Laboratories (WACL), Department of Chemistry,
7 University of York, Heslington, York, YO10 5DD, UK.

8 ²Instituto Nacional de Meteorologia e Geofísica, São Vicente (INMG), Mindelo, Cabo Verde.

9 ³National Centre for Atmospheric Science (NCAS), University of York, Heslington, York,
10 YO10 5DD, UK.

11 ⁴FAAM Airborne Laboratory, Building 146, Cranfield University, Cranfield, MK43 0AL, UK.

12 *Corresponding author: sta516@york.ac.uk

13

14



15 Abstract

16 Atmospheric nitrogen oxides ($\text{NO} + \text{NO}_2 = \text{NO}_x$) have been measured at the Cape Verde
17 Atmospheric Observatory (CVAO) in the tropical Atlantic ($16^\circ 51' \text{ N}$, $24^\circ 52' \text{ W}$) since
18 October 2006. These measurements represent a unique time series of NO_x in the background
19 remote troposphere. Nitrogen dioxide (NO_2) is measured via photolytic conversion to nitric
20 oxide (NO) by ultra violet light emitting diode arrays followed by chemiluminescence
21 detection. Since the measurements began, a “blue light converter” (BLC) has been used for
22 NO_2 photolysis, with a maximum spectral output of 395 nm from 2006-2015 and of 385 nm
23 from 2015. The original BLC used was constructed with a Teflon-like material and appeared
24 to cause an overestimation of NO_2 when illuminated. To avoid such interferences, a new
25 additional photolytic converter (PLC) with a quartz photolysis cell (maximum spectral output
26 also 385 nm) was implemented in March 2017. Once corrections are made for the NO_2 artefact
27 from the original BLC, the two NO_2 converters are shown to give comparable NO_2 mixing
28 ratios ($\text{PLC} = 0.92 \times \text{BLC}$, $R^2 = 0.92$), giving confidence in the quantitative measurement of
29 NO_x at very low levels. Data analysis methods for the NO_x measurements made at CVAO have
30 been developed and applied to the entire time series to produce an internally consistent and
31 high quality long-term data set. NO has a clear diurnal pattern with a maximum mixing ratio
32 of 2-10 pptV during the day depending on the season and ~ 0 pptV during the night. NO_2 shows
33 a fairly flat diurnal signal, although a small increase in daytime NO_x is evident in some months.
34 Monthly average mixing ratios of NO_2 vary between 5 and 30 pptV depending on the season.
35 Clear seasonal trends in NO and NO_2 levels can be observed with a maximum in autumn/winter
36 and a minimum in spring/summer.

37

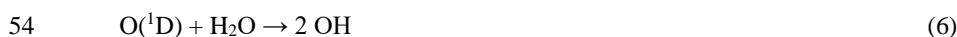


38 1 Introduction

39 Atmospheric nitrogen oxides play a key role in tropospheric chemistry. NO_x helps to
40 control the abundance of the two most important oxidants in the atmosphere, ozone (O₃) and
41 the hydroxyl radical (OH). The presence of NO is usually the key limiting factor in the
42 production of tropospheric O₃, which occurs via oxidation of NO to NO₂ by peroxy radicals
43 (RO₂, HO₂) as described in reactions (1-2), followed by photolysis of NO₂ and rapid conversion
44 of the resulting O(³P) to O₃:



49 Reaction (2) also offers a route to the OH radical, above its primary production via O₃
50 photolysis (reactions (5) and (6)). If the NO_x mixing ratio is sufficiently low, then peroxy
51 radicals react with themselves instead of NO, and O₃ depleting reactions (reactions (5) to (8))
52 dominate over O₃ production (Atkinson, 2000).



57 NO_x mixing ratios below 10-30 pptV are generally sufficiently low for net tropospheric O₃
58 depletion (Atkinson, 2000; Jaeglé et al., 1998; Logan, 1985). These conditions have previously
59 been reported to apply most of the year in the remote Atlantic Ocean (Lee et al., 2009). The
60 mixing ratio of NO_x in the atmosphere varies from a few pptV in remote areas (Lee et al., 2009;
61 Monks et al., 1998; Reed et al., 2017) to >100 ppbV in polluted areas (Carslaw, 2005; Mazzeo
62 et al., 2005; Pandey et al., 2008). It is therefore important to have representative NO_x
63 measurements in different regions of the world to be able to understand the chemistry occurring
64 throughout the troposphere.

65 Long-term remote atmospheric NO_x measurements are rare due to the difficulty measuring
66 very low (pptV) mixing ratios. Many different methods of measuring NO_x are available,



67 however, very few have the limit of detection (LOD) and sensitivity needed to measure NO_x
68 in remote regions. The most widely used method is NO chemiluminescence, where NO in the
69 presence of excess ozone is oxidized into excited state NO_2 , which emits photons that can be
70 detected (Fontijn et al., 1970). NO_2 is generally converted into NO either catalytically by a
71 heated molybdenum converter or photolytically, followed by NO chemiluminescence (Kley
72 and McFarland, 1980). The molybdenum converter has historically been preferred due to its
73 high conversion efficiency of at least 95%, but it also converts other reactive nitrogen species
74 (NO_z) such as peroxyacetyl nitrate (PAN), peroxyethacryloyl nitrate (MPAN), acyl peroxy
75 nitrates (APN), HNO_3 , p- HNO_3 , and HONO, potentially giving an overestimation of NO_2
76 (Dunlea et al., 2007; Grosjean and Harrison, 1985; Winer et al., 1974). Two separate studies
77 have shown that photolytic converters (PLC) with a wavelength of 385-395 nm have the
78 smallest spectral overlap with interfering compounds (Pollack et al., 2010; Reed et al., 2016).
79 Reed et al., (2016) showed that in some configurations the PLC can heat up the sampled air
80 making it possible for reactive nitrogen compounds such as peroxyacetyl nitrate (PAN) to
81 decompose thermally and cause an overestimation of NO_2 . This, however, causes only a
82 negligible interference in warm regions such as Cabo Verde where PAN levels are extremely
83 low (Reed et al., 2016).

84 In this study we describe a NO_2 converter, similar to that presented by Pollack et al. (2010),
85 which has been implemented on an instrument to measure NO_x at the CVAO. The data analysis
86 procedure is explained in detail and the first two years of results with the new converter are
87 presented and compared to the data obtained using a different converter.

88

89 2 Experimental

90 2.1 Location

91 The Cape Verde Atmospheric Observatory (CVAO; 16° 51' N, 24° 52' W) is located on
92 the north eastern coast of São Vicente, Cabo Verde. The air masses arriving at the CVAO
93 predominately come from the northeast (>95% of all wind direction measurements, see Figure
94 1) and have travelled over the Atlantic Ocean for multiple days since their last exposure to
95 anthropogenic emissions, with the potential exception of ship emissions (Carpenter et al., 2010;
96 Read et al., 2008). The UK Meteorological Office NAME dispersion model (Ryall et al., 2001)
97 has previously been used to investigate the origin of the air masses arriving at the CVAO,

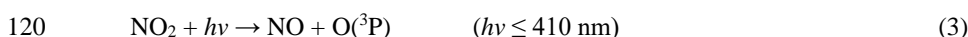
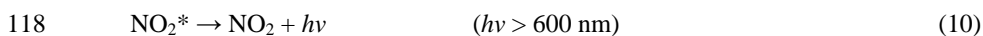


98 which have been shown to be very diverse; North America, the Atlantic, Europe, Arctic, and
99 African regions (Lee et al., 2009). During the spring and summer, the air masses predominantly
100 originate from the Atlantic making it possible to investigate long-term remote marine
101 tropospheric background measurements. During the winter, the CVAO receives air mainly
102 from the Sahara, resulting in very high wintertime dust loadings (Chiapello et al., 1995; Fomba
103 et al., 2014; Rijkens et al., 2008). The time zone of Cabo Verde is always UTC-1. A full
104 description of the CVAO site and associated measurements is given in Carpenter et al. (2010).

105

106 2.2 Measurement Technique

107 NO_x has been measured at the CVAO since 2006 using a NO_x chemiluminescence
108 instrument manufactured by Air Quality Design Inc. (AQD), USA. The chemiluminescence
109 technique involves the oxidation of NO by excess O_3 to excited NO_2 (Reaction 9) (Clough and
110 Thrush, 1967; Clyne et al., 1964; Fontijn et al., 1970). The excited NO_2 molecules can be
111 deactivated by emitting photons or by being quenched by other molecules (Reaction 10 and
112 11) such as N_2 , O_2 , and in particular H_2O . The emitted photons are detected by a
113 photomultiplier tube detector (PMT), which gives a signal linearly proportional to the mixing
114 ratio of NO sampled. The measurement of NO_x and NO_2 requires photolytic conversion of NO_2
115 to NO (Reaction 3) followed by NO chemiluminescence detection (Kley and McFarland,
116 1980).



121 Further details of the technique are documented in (Carpenter et al., 2010; Drummond et al.,
122 1985; Fontijn et al., 1970; Lee et al., 2009; Peterson and Honrath, 1999; Reed et al., 2017; Val
123 Martin et al., 2006).

124



125 2.3 Instrument Set-up

126 Ambient air is sampled from a downward facing inlet placed into the prevailing wind with
127 a fitted hood 10 m above the ground. A centrifugal pump at a flow rate of ~750 litres per minute
128 pulls the air into a 40 mm glass manifold resulting in a linear sample flow of 10 m s^{-1} , giving
129 a residence time to the inlet of the NO_x instrument of 2.3 s. To reduce the humidity and aerosol
130 concentration in the sampled air, dead-end traps are placed at the lowest point of the manifold
131 inside and outside the laboratory. A Nafion dryer (PD-50T-12-MKR, Permapure) is used to
132 additionally dry the sampled air, using a constant sheath flow of zero air (PAG 003, Eco Physics
133 AG) that has been filtered through a Sofnofil (Molecular Products) and activated charcoal
134 (Sigma Aldrich) trap (dewpoint -15°C). The air is sampled perpendicular to the manifold
135 through a 47mm PTFE (polytetrafluoroethylene) filter with a pore size of $1.2 \mu\text{m}$.

136 A schematic diagram of the instrument is shown in Figure 2. Sampled air is passed through
137 two different photolytic NO_2 converters, which are placed in series. The first is a commercial
138 unit known as a BLC (Blue Light Converter) supplied by Air Quality Design, as described in
139 (Buhr, 2007). An ultra violet light emitting diode (UV-LED, 3 W, LED Engin, Inc.) array is
140 placed in each end of a reaction chamber made of Teflon-like barium doped material (BLC, λ
141 $= 385 \text{ nm}$, volume $= 16 \text{ cm}^3$). The entire block surrounding the reaction chamber is irradiated,
142 giving the highest possible conversion efficiency of NO_2 . Each array is cooled by a heat sink
143 to maintain an approximately constant temperature inside of the converter when the diode
144 arrays turn on. The second converter consists of two diodes (Hamamatsu Lightningcure
145 L11921-500, $\lambda = 385 \text{ nm}$) and a photolysis cell made of a quartz tube and two quartz windows
146 glued to each end with a volume of 16 cm^3 (PLC) following the design of Pollack et al. (2010).
147 Aluminium foil is wrapped around the quartz tube to increase the reflectivity to give the highest
148 conversion efficiency of NO_2 . The diodes are placed at each end of the quartz tube, as shown
149 in Figure S2, without touching the windows to avoid increases in the temperature when the
150 diodes turn on. BLCs have been used at the CVAO since the instrument was installed in 2006,
151 with the most recent converter installed in April 2015 (a BLC2 model), where the wavelength
152 was changed to 385 nm from 395 nm. The PLC was installed in March 2017. The air flow
153 through the instrument is controlled at $\sim 1000 \text{ sccm}$ by a mass flow controller (MKS, M100B)
154 giving a residence time of 0.96 s through each of the converters.

155 To measure NO and NO_x ($\text{NO} + \text{NO}_2$ converted into NO) the air is introduced to the
156 chemiluminescent detector (CLD), where NO is oxidized by excess O_3 into excited NO_2 in the



157 reaction volume (241 mL, aluminium with gold coating (Ridley and Grahek, 1990)) shown in
158 Figure 2. The reaction volume is kept at low pressure to minimize quenching of excited NO₂
159 and thereby maximize the NO chemiluminescence lifetime. The photons emitted from the
160 excited NO₂ molecules when they relax to ground state are detected by the PMT (Hamamatsu
161 R2257P) to give a signal for NO. NO₂ is converted into NO by the BLC for 1 minute, and then
162 the PLC for 1 minute, each period producing a signal due to NO + NO₂. The signal detected
163 by the PMT (S_M) is caused by NO reacting with O₃ (S_{NO}), dark current from the thermionic
164 emissions from the photocathode of the PMT (S_D), and an interference (S_I) which can be due
165 to other gas-phase reactions creating chemiluminescence and from illumination of the chamber
166 walls during NO₂ conversion (Drummond et al., 1985; Reed et al., 2016):

$$167 \quad S_M = S_{NO} + S_D + S_I \quad (I)$$

168 The PMT is cooled to -30°C to reduce the dark current, giving the instrument a higher
169 precision. Other molecules in the atmosphere such as alkenes also react with ozone and emit
170 photons to reach their ground state, but at a different time-scale to that of NO₂ (Alam et al.,
171 2020; Finlayson et al., 1974). This can give an interfering signal causing the NO and NO_x
172 mixing ratios to be overestimated. However, most of these reactions emit photons at 400-600
173 nm and are therefore filtered by a red transmission cut-off filter (Schott RG-610) placed in
174 front of the PMT (Alam et al., 2020). The filter transmits photons with a wavelength higher
175 than 600 nm (Drummond et al., 1985). A background measurement is therefore required to
176 account for the dark current of the PMT and for the remaining interfering reactions occurring
177 at a different time-scale to that of NO₂. Background measurements are made by allowing
178 ambient air to interact with O₃ in the zero volume (180 mL, PFA, Savillex, LLC) before
179 reaching the reaction volume (Figure 2). Most excited NO₂ molecules will reach their ground
180 state before the sample reaches the PMT, meaning the signal from NO will not be measured.
181 The efficiency of the reaction between NO and O₃ in the zero volume is calculated from the
182 calibration and will be explained in section 2.4.3.

183 NO, NO₂ and the background signal are all detected on the same channel, and the
184 instrument cycle is 1 min of background, 2 min of NO (when the NO₂ converters are off), 1
185 min of BLC NO_x (the BLC converter is on), and 1 min of PLC NO_x (the PLC is on).

186



187 2.4 Calibration

188 Prior to June 2019, calibrations were performed every 73 hours by standard addition in
189 order to account for temperature and humidity changes in the ambient matrix. In June 2019 the
190 calibration frequency was changed to every 61 hours to ensure that during any given month,
191 calibrations are carried out for approximately equal periods during the night and the day. To
192 calibrate the NO sensitivity, 8 sccm of 5 ppmV NO calibration gas in nitrogen is added to the
193 ambient air flow of ~1000 sccm, giving an NO mixing ratio of approximately 40 ppbV. The
194 mixing ratio used for calibrations are approximately 10,000 times that of the ambient
195 measurements, however, due to reduced cylinder stability for lower NO mixing ratios it is
196 difficult to calibrate at much lower mixing ratios and the chemiluminescence is expected to be
197 linear across the range of expected mixing ratios (Drummond et al., 1985). The calibration gas
198 is added between the PTFE filter and the NO₂ converter as shown in Figure 2. The conversion
199 efficiency of the BLC and the PLC is calibrated by gas phase titration (GPT), where oxygen is
200 added to the sampled NO calibration gas before entering the titration cell, which contains a UV
201 lamp that converts oxygen to ozone. Between 60-80% of the NO calibration gas is oxidized
202 into NO₂, giving a known mixing ratio of NO₂. A theoretical calibration sequence is shown in
203 Figure 3. The first cycle is to calibrate the sensitivity and the second is to calibrate the NO₂
204 conversion efficiency. Each actual calibration includes three cycles of sensitivity calibration
205 and two cycles of conversion efficiency calibration. The signal from NO₂ observed in the NO
206 sensitivity calibration is due to traces of NO₂ in the calibration gas. Figure S3 shows the
207 observed percentage of NO₂ in the calibration cylinders from January 2014 to August 2019
208 calculated from the measured sensitivity (sec. 2.4.1) and the conversion efficiencies (CE) of
209 the two converters (sec. 2.4.2):

$$210 \quad \text{NO}_2 \text{ in cylinder (pptV)} = \frac{(\text{NO}_{c(1)} - \text{NO}_{(1)})}{\text{Sensitivity} \times \text{CE}} \quad (\text{II})$$

$$211 \quad \text{Percentage NO}_2 = \frac{\text{NO}_2 \text{ in cylinder}}{\text{NO}_2 \text{ in cylinder} + \text{NO cal conc.}} \quad (\text{III})$$

212 The percentage is stable for both converters, however, the PLC shows approximately 3-
213 4% NO₂ in the NO calibration gas compared to 5-10% for the BLC, which is caused by a BLC
214 artefact. The cylinders used were certified to ≤2% NO₂.

215



216 2.4.1 Sensitivity

217 The sensitivity of the instrument is calculated from the increase in counts per second
218 caused by the calibration gas during NO calibration (untitrated, i.e. without O₃) and from the
219 mixing ratio of the calibration gas as shown by equation (IV). The NO counts per second from
220 the previous measurement cycle before the calibration is subtracted to give the increase due to
221 the calibration gas. The previous cycle needs to be stable and low in NO to give an accurate
222 sensitivity, which is the case at the CVAO.

$$223 \quad \text{Sensitivity} = \frac{\text{Counts per second during calibration} - \text{Counts per second in previous cycle}}{\text{Mixing ratio of calibration gas}} \quad (\text{IV})$$

224 The sensitivity of the instrument depends on the pressure of the reaction chamber, the
225 ozone mixing ratio in the reaction chamber, the flow of the sample through the reaction
226 chamber, and the temperature of the reaction chamber. To maintain a stable sensitivity, all four
227 parameters should be kept stable (Galbally, 2019). From January 2014 to August 2019 the
228 sensitivity has varied between 2.7 and 7.4 counts s⁻¹ pptV⁻¹ with changes of less than 5%
229 between subsequent calibrations (see Figure S4), unless the instrument has been turned off for
230 a long period of time due to instrumental problems.

231

232 2.4.2 Conversion Efficiencies

233 The conversion efficiency of the BLC and the PLC is calculated based on the titrated (with
234 added O₃) and the untitrated (without added O₃) NO calibration gas as described in equation
235 (V). The numerator gives how much of the NO is titrated into NO₂ and the denominator
236 represents the NO₂ measured when taking the NO₂ content in the NO calibration gas into
237 account. In equation (V), “NO” is the measurement of only NO i.e. when the converters are
238 off, NO.c is when one of the converters are on therefore the measurement is NO + NO₂ and (1)
239 and (2) represent untitrated and titrated NO, respectively.

$$240 \quad \text{CE} = \frac{[(\text{NO.c}_{(2)} - \text{NO}_{(2)}) - (\text{NO.c}_{(1)} - \text{NO}_{(1)})]}{[\text{NO}_{(1)} - \text{NO}_{(2)}]} = 1 - \frac{\text{NO.c}_{(1)} - \text{NO.c}_{(2)}}{\text{NO}_{(1)} - \text{NO}_{(2)}} \quad (\text{V})$$

241 The conversion efficiency of the BLC has varied from 82% to 91% between its installation in
242 April 2015 and August 2019 ($j \sim 3 \text{ s}^{-1}$). Prior to April 2015, an older generation BLC ($\lambda = 395$
243 nm) with a conversion efficiency of 30-35% was used ($j \sim 0.5 \text{ s}^{-1}$). The conversion efficiency
244 of the PLC has varied between 50% and 55% from its installation in March 2017 to August
245 2019 ($j \sim 1 \text{ s}^{-1}$). See Figure S5 for all the calculated conversion efficiencies.



246

247 2.4.3 Efficiency of the Zero Volume

248 Background measurements are made by reacting NO and interference compounds with O₃
249 in the zero volume (Figure 2). The system is set up so that NO₂ produced from NO will relax
250 to the ground state before it is measured in the downstream reaction chamber, whereas it is
251 assumed that any interfering compounds will emit photons when reaching the reaction chamber
252 and be measured as a background signal (Drummond et al., 1985; Galbally, 2019). If the zero
253 volume is too small or the O₃ mixing ratio is too low, some untitrated NO may lead to NO₂
254 chemiluminescence within the reaction chamber and the background will be overestimated. On
255 the other hand, if the zero volume is too large, some of the interfering compounds may have
256 relaxed to their ground state before the reaction chamber and the background signal will be
257 underestimated. The residence time of zero volume is 10.8s compared to 14.5s for the reaction
258 volume. The efficiency of the zero volume can be calculated from the calibration cycle. The
259 difference in background counts from before a calibration cycle to during the calibration cycle
260 shows how much of the added NO from the calibration cylinder does not react with O₃ in the
261 zero volume. By dividing this difference by the signal due to NO during the NO measurement
262 of the calibration cycle, which is obtained by subtracting the NO measurement from the
263 previous measurement cycle, the inefficiency of the zero volume is obtained. The efficiency is
264 determined for each calibration cycle (eq. VI) and plotted in Figure S6. It is consistently above
265 98%.

$$266 \quad \text{Efficiency}_{ZV} = 1 - \frac{\text{cal zero} - \text{measurement zero}}{\text{NO cal} - \text{previous NO cycle}} \quad (\text{VI})$$

267

268 2.4.4 Artefact Measurements

269 As described in section 2.3, NO_x measurements may have artefacts from
270 chemiluminescence caused by interfering gas-phase reactions and/or from compounds
271 produced by illumination of the reaction chamber walls as well as from pressure differences in
272 the instrument (Drummond et al., 1985; Reed et al., 2016). To estimate artefacts, it is necessary
273 to measure the signal from NO_x-free air. The calibration sequence is followed by sampling
274 NO_x-free air generated from a pure air generator (PAG 003, Eco Physics AG) for 30 minutes.
275 According to the manufacturer, the PAG not only scrubs NO, NO₂ and NO_y from the ambient
276 air but also SO₂, VOCs, H₂O and O₃. An overflow of PAG air is introduced between the aerosol



277 filter and the NO₂ converters as shown in Figure 2 and the cycle of background, NO, NO_x BLC,
278 and NO_x PLC is used to estimate artefact NO and NO₂ measured by the instrument.

279

280 2.4.4.1 NO Artefact

281 The NO artefact can be caused by two things; alkenes reacting with O₃ and giving
282 chemiluminescence above 600 nm at approximately the same rate as NO₂ or a difference in
283 pressure between the zero volume and the reaction volume. An artefact caused by alkenes will
284 be positive and overestimate the NO mixing ratio, where an artefact due to a pressure difference
285 can be either negative or positive. It can be estimated as the offset from 0 pptV when the mixing
286 ratio sampled is 0 pptV. The NO mixing ratio is expected to be 0 pptV when sampling NO_x-
287 free air or between 22.00 and 04.00 UTC at night. NO generated during the day is rapidly
288 oxidized into NO₂ through reactions with O₃ and RO₂ after sunset. During the night, NO is not
289 generated from photolysis of NO₂, and there are no significant local sources of NO at Cabo
290 Verde when the air masses come from over the ocean (which is >95% of the time). The average
291 NO mixing ratio between 22.00 and 04.00 UTC and the average NO mixing ratio from the
292 PAG zero air tend to be very similar, with the PAG artefact (-3.68 ± 22.91 pptV (2σ), January
293 2014 – August 2019) ordinarily lower than the night time artefact (0.39 ± 11.92 pptV (2σ),
294 January 2014 – August 2019). Time series of both NO artefact measurements can be found in
295 Figure S7 in the supplementary information. The night time NO artefact is used as it is
296 measured more frequently, it contains the same ambient matrix with nothing scrubbed and to
297 eliminate the possibility of residual NO influencing background measurements determined
298 from the PAG. Since the PAG scrubs VOCs it will also not give an estimate of the artefacts
299 caused by fast reacting alkenes.

300

301 2.4.4.2 NO₂ Artefact

302 NO₂ converters have previously been shown to have artefacts caused by thermal or
303 photolytic conversion of reactive nitrogen compounds (NO₂) other than NO₂ as well as
304 illumination of the chamber walls (Drummond et al., 1985; Reed et al., 2016; Ryerson et al.,
305 2000). Fast reacting alkenes, which can cause overestimations of the NO mixing ratios, will
306 not cause the NO₂ mixing ratio to be overestimated, since the NO signal is subtracted from the
307 NO₂ signal.



308 The spectral output of an NO₂ converter with a wavelength of 385 nm was compared to
309 absorption cross sections of NO₂ and potential interfering species such as BrONO₂, HONO and
310 NO₃ (Reed et al., 2016). The photolytic converter was shown to have good spectral overlap
311 with the NO₂ cross section with minimal spectral overlap with other NO_z species, except for a
312 small overlap with the absorption cross section of HONO. The interference from BrONO₂,
313 HONO and NO₃ have additionally been evaluated previously for a similar set-up using a Hg
314 lamp (Ryerson et al., 2000). At equal concentrations of NO₂ and NO_z species, BrONO₂ and
315 NO₃ were estimated to maximum have an interference of 5% and 10%, respectively, using a
316 lamp with a wider spectral overlap with the interfering species than what is observed for the
317 LEDs used at the CVAO (Ryerson et al., 2000). At the CVAO, HONO levels have previously
318 been measured to peak at ~3.5 pptV (at noon; (Reed et al., 2017)). For the typical Gaussian
319 output of a UV-LED this interference is calculated to be 2.0, 12.6, and 25.7% for UV-LEDs
320 with principle outputs of 395, 385, and 365 nm respectively, resulting in a maximum
321 interference of <0.5 pptV during peak daylight hours. Photolytic conversion of NO_z species is
322 therefore not expected to be an important contributor to the NO₂ artefact at the CVAO due to
323 the narrow spectral output of the LEDs.

324 Each converter is only on for 1 minute in a 5-minute cycle. For thermal conversion to be
325 a major contributor to the artefact, the converter would have to increase in temperature during
326 that one minute and not the rest of the cycle otherwise an increase in signal should be constant
327 since the air continues to flow through the converters when they are turned off. Thermal
328 decomposition of NO_z species is therefore not expected to have an effect in a climate like the
329 one in Cabo Verde, where the sample temperatures are similar to the ambient temperatures.

330 It has been shown that the walls of a BLC made out of a porous Teflon-like doped block
331 becomes contaminated from the ambient air over time and when the walls are illuminated
332 reactions take place on the surface causing an artefact (Reed et al., 2016; Ryerson et al., 2000).
333 The BLC is similar to the one used by Reed et al. (2016) and it is therefore expected to have
334 an artefact due to reactions taking place on the surface. The PLC is not expected to be
335 contaminated in the same way as it does not have porous chamber walls. Ryerson et al. (2000)
336 observed an increase in artefact over time when sampling ambient air for a similar PLC,
337 however, this is not observed for the PLC in the very clean environment at the CVAO (0-10
338 pptV between August 2017 and August 2019, see below) and surface reactions are therefore
339 expected to give a negligible artefact for the PLC.



340 The total artefact can be determined by measuring the NO₂ signal when the NO₂ mixing
341 ratio is 0 pptV, however, it is virtually impossible to scrub all NO_x from the ambient air and
342 nothing else. To estimate the NO₂ artefact, PAG zero air is measured using both converters.
343 The PLC measures between 0-10 pptV compared to 10-60 pptV using the BLC. Since, as
344 discussed above, the NO₂ artefact of the PLC is believed to be negligible, the signal is believed
345 to represent the remaining NO₂ in the zero air after scrubbing. The signal from the BLC when
346 measuring PAG zero air is expected to be due to the illumination of the chamber walls in
347 addition to the traces of NO₂ left in the zero air. The artefact due to wall reactions in the BLC
348 can therefore be estimated by subtracting the signal measured by the PLC.

349

350 3 Data Analysis

351 Time periods with known problems such as maintenance on the manifold, ozone leaks,
352 and periods when the PMT has not reached <-28°C are not included in the dataset. The mean
353 and standard deviation of the zero (background), NO, NO₂ BLC and PLC are determined for
354 each 5-minute measurement cycle. To avoid averaging over the time it takes the detector to
355 change and stabilize between the different types of measurements, the last 50 seconds of the
356 measurement cycle are used for the background and the NO counts, and the last 30 seconds for
357 the BLC NO_x and the PLC NO_x counts. Each cycle is filtered based on the percentage standard
358 deviations and differences in counts between subsequent cycles. If the standard deviation or
359 the difference in counts are outside the mean ± 2σ (see Table 1) calculated from a 5-year period
360 between 2014 and 2018, the cycle is not used for further analysis. This removes noisy data as
361 well as sharp spikes but keeps data with sustained increases lasting more than 5 minutes.

362 To obtain the signals due to NO and NO₂, the interpolated zero and NO measurements are
363 subtracted from the NO and NO_x measurements, respectively. They are converted to a
364 concentration by using the interpolated sensitivity and conversion efficiency as shown in
365 equation VII and VIII:

$$366 \quad \text{NO mixing ratio} = \frac{\text{NO measurement} - \text{background measurement}}{\text{Sensitivity}} \quad (\text{VII})$$

$$367 \quad \text{NO}_2 \text{ Mixing ratio} = \frac{\text{NO}_x \text{ measurement} - \text{NO measurement}}{\text{Sensitivity} \times \text{CE}} \quad (\text{VIII})$$

368 The NO and NO₂ BLC concentrations are corrected by subtracting the interpolated
369 artefacts described in sections 2.4.4.1 and 2.4.4.2. If the difference between two subsequent



370 NO artefact measurements vary by more than the mean $\pm 2\sigma$ of the differences in NO artefacts
371 determined from January 2014 – August 2019 (0.00 ± 6.18 pptV), the measurements made
372 between will not be used for further analysis due to a potential step change between the
373 determinations.

374 Hourly averages of all the measurements are determined. If data coverage during the hour
375 is less than 50%, the hour is flagged and discarded from the data analysis. The hourly NO_x (NO
376 + NO₂ PLC) concentrations between June 2017 and August 2019 are plotted as a function of
377 wind speed and direction in figure 4. It can be observed that the concentrations are enhanced
378 at low wind speed and when the air crosses the island (southwest). Measurements made at a
379 wind speed <2 m/s or from a wind direction $>100^\circ$ are, therefore, flagged as suspected of local
380 contamination and are not used in the analysis. Extreme mixing ratios outside the mean $\pm 4\sigma$
381 of the 5-year for NO and 2-year period for NO₂ are flagged as suspicious (see Table 1 for
382 boundaries). Lastly, inconsistency in the measurements such as differences outside the mean \pm
383 4σ between the mean and median of a measurement (see Table 1 for boundaries) and
384 differences between the two NO₂ measurements are flagged as suspicious (0.4 ± 32.2 pptV).
385 The data remaining after these removals are 88% of the original NO and NO₂ BLC dataset and
386 83% of the NO₂ PLC dataset remain to analyse.

387

388 3.1 Corrections

389 As described above, excited NO₂ can be quenched by other sampled molecules, giving a
390 lower observed mixing ratio than the real value. Water molecules are effective quenchers and
391 therefore a correction is usually applied depending on the humidity (Matthews et al., 1977;
392 Ridley et al., 1992). However, since the calibrations at the CVAO are performed by standard
393 addition, and a Nafion dryer is placed in front of the instrument, this is not necessary.

394 Additionally, NO can react with O₃ in the ambient air in the inlet and manifold giving an
395 overestimation of NO₂ and an underestimation of NO. To correct for this the following
396 equations are used (Gilge et al., 2014):

$$397 \quad [\text{NO}]_0 = [\text{NO}]_{\text{E1}} \times e^{k_{\text{O}_3} \times t_{\text{E1}}} \quad (\text{IX})$$

$$398 \quad [\text{NO}_2]_0 = \left(\frac{J_{\text{C}} + k_{\text{O}_3}}{J_{\text{C}}} \right) \times \left(\frac{[\text{NO}]_{\text{E2}} - [\text{NO}]_{\text{E1}} \times e^{-(k_{\text{O}_3} \times (t_{\text{C2}} - t_{\text{C1}}) + J_{\text{C}} \times t_{\text{C2}})}}{1 - e^{-(k_{\text{O}_3} + J_{\text{C}}) \times t_{\text{C2}}}} \right) - [\text{NO}]_0 \quad (\text{X})$$



399 where $[\text{NO}]_0$ is the corrected NO mixing ratio, $[\text{NO}]_{\text{E1}}$ is the uncorrected NO mixing ratio,
400 $[\text{NO}_2]_0$ is the corrected NO₂ mixing ratio, $[\text{NO}]_{\text{E2}}$ is the uncorrected NO mixing ratio when the
401 converter is on, k_{O_3} is the rate of the reaction between NO and O₃ ($k(\text{O}_3+\text{NO}) \times [\text{O}_3] \times 10^{-9} \times$
402 M), t_{E1} is the sum of the residence time from the inlet to entry of the converter and the time the
403 air is in the converter, t_{C1} and t_{C2} are the time the air is in the converter when the converter is
404 on and off, respectively, and J_{C} is the photolysis rate inside the converter. The residence time
405 from the inlet to the entry of the converter has been 2.3 s since 2015 and the time the air is in
406 each of the converters is 1.0 s (with and without the converter on). The O₃ mixing ratio
407 measured at the CVAO has varied between 5 and 60 ppbV (with an uncertainty of 0.07 ppbV)
408 between 2014 and 2019. The ozone correction is calculated for each hour using a rate
409 coefficient of $1.8 \times 10^{-14} \text{ cm}^3 \text{ molecule}^{-1} \text{ s}^{-1}$ at 298K (Atkinson et al., 2004). This gives an
410 average O₃ correction $\pm 2\sigma$ of $6.8 \pm 3.0\%$, $1.7 \pm 11.0\%$, and $1.3 \pm 7.1\%$ for NO, NO₂ BLC, and
411 NO₂ PLC, respectively, when the mixing ratio measured is above 0.1 pptV (See supplementary
412 information for an example of the calculation). Thus, at the low mixing ratios of O₃ present at
413 Cabo Verde and the short residence time for sampling, the corrections for O₃ are well within
414 the noise of the measurements (see below), but are still included in the final calculated mixing
415 ratios.

416

417 4 Uncertainty Analysis

418 To be able to evaluate the NO_x measurements made at the CVAO an extensive uncertainty
419 analysis is performed. A summary of the analysis can be found in Table 2 and a detailed
420 description in the supplementary information. The hourly precision and uncertainty of the
421 instrument are estimated to characterize the uncertainties at the 95 percent confidence interval
422 (Bell, 1999). The hourly precision is estimated from the zero count variability, which is directly
423 related to the photon-counting precision of the PMT. The uncertainty of the hourly
424 measurements is estimated by combining all the uncertainties associated with the
425 measurements. This includes uncertainties in the calibrations, artefact determinations, and O₃
426 corrections as well as the precision of the instrument. The precision of the NO and NO₂
427 measurements are both included in the total uncertainty of the NO₂ measurements as the NO
428 measurements are subtracted from the NO₂ measurements. Each term is converted into pptV
429 to be able to combine them using error propagation.



430 The 2σ precision for hourly averaged NO data between January 2014 and August 2019 is
431 0.96 ± 0.89 pptV. The hourly precisions reported here are in good agreement with our
432 previously reported 1σ precision of the instrument of 0.30 pptV (Reed et al., 2017) and the 2σ
433 precision of 0.6-1.7 pptV (Lee et al., 2009). The NO₂ precisions are determined by taking the
434 conversion efficiency of the respective converters into account. The hourly 2σ precision for
435 hourly averaged NO₂ data between March 2017 and August 2019 becomes 1.45 ± 0.82 pptV
436 and 2.74 ± 2.18 pptV for the BLC and PLC, respectively. The determined NO₂ precisions are
437 within the interval of previously reported precisions for the same instrument (Lee et al., 2009;
438 Reed et al., 2017).

439 The total hourly uncertainty for each of the three measurements are determined by
440 combining all the uncertainties described using propagation of uncertainties. The precisions
441 are already calculated as hourly precisions in pptV. The calibration uncertainties are
442 interpolated between each calibration and multiplied by the hourly concentrations of NO and
443 NO₂ to calculate hourly uncertainties in pptV. The artefact uncertainties are interpolated
444 between each artefact determination, and the uncertainty due to ozone corrections is determined
445 by multiplying the % uncertainties by the hourly concentrations of NO and NO₂. The hourly
446 uncertainties are determined to be 1.42 ± 1.47 pptV, 8.38 ± 7.46 pptV, and 4.44 ± 5.79 pptV
447 for NO, NO₂ BLC, and NO₂ PLC, respectively.

448

449 5 Results: Examples of Data

450 The first year of data (August 1st 2017 to July 31st 2018) is chosen as an example of the
451 resulting NO and NO₂ datasets. October 2017, December 2017, and April 2018 are used to
452 highlight the seasonality in the mixing ratios observed during a year of measurements. Panel
453 A in figure 5 and 6 show the full O₃ corrected time series for NO and NO₂, respectively. Panel
454 B, C, and D in the two figures show the time series for the three chosen months and panel E,
455 F, and G show the 3-hour rolling average diurnals for the same months. Monthly diurnals for
456 NO and NO₂ for the entire year can be found in figure S8 and S9, respectively.

457 Clear seasonality can be observed in the diurnal cycles of NO measurements with a
458 maximum of ~ 10 pptV in Winter and a minimum of ~ 2 pptV in the spring and summer. This
459 is in good agreement with that reported for previous years (Lee et al., 2009; Reed et al., 2017).
460 The two NO₂ measurements are in general in good agreement when looking at the time series



461 in figure 6. Offsets of up to 10 pptV between the two measurements can be seen over some
462 time periods (E.g. April, Panel D), which are most likely caused by the calculated BLC artefact
463 for those periods either being too high or too low. This is supported by the diurnals having the
464 same shape, but with an offset. Monthly diurnals of the two NO₂ measurements agree within 2
465 standard errors except in August 2017, where the offset between the two measurements is larger
466 than for the remaining months. NO₂ shows a fairly flat diurnal signal, although a small increase
467 in daytime NO₂ is evident in some months, which is in agreement with that reported for
468 previous years (Lee et al., 2009; Reed et al., 2017). Spikes in the early morning are noticeable
469 in the NO₂ diurnals for July-November, which correspond to the months with an average lower
470 wind speed than the rest of the year (the diurnal for April also shows a spike, however, it is
471 caused by only one morning). These spikes could be caused by local fishing boats passing
472 upwind of the observatory in the morning hours, which will give a more prominent spike a low
473 wind speed. Monthly wind speed diurnals can be found in figure S10. The good agreement
474 between the two NO₂ measurements observed in figure 6 can also be observed in figure 7,
475 where the two are plotted against each other. The data points are scattered around the 1:1 line
476 shown in black with an overestimation by the BLC. An orthogonal distance regression (ODR)
477 is performed to evaluate the scatter of the data points with uncertainty in both measurements
478 between August 2017 and 2019. The resulting regression line is displayed in red (PLC NO₂ =
479 $0.92 \times \text{BLC NO}_2$, $R^2 = 0.92$).

480 The seasonality of the NO measurements can be explained by a combination of the
481 variation of the origin of the air masses arriving at the CVAO, meteorology, photolysis rates,
482 and seasonality of emissions. Back trajectories of the three months used as examples are shown
483 in figure 8. FLEXPART version 10.4 is used in backwards mode, driven by pressure level data
484 from Global Forecast System (GFS) reanalyses at 0.5°×0.5° resolution (Pisso et al., 2019; Stohl
485 et al., 1998). 10-day back-trajectory simulations are initialised every 6 hours, releasing 1000
486 particles from the CVAO site. Further information on FLEXPART can be found in the
487 supplementary information. During the winter maximum (December) the back-trajectories
488 indicate that the air reaching CVAO is largely dominated by African air, compared to during
489 the spring minimum (April), which is dominated by Atlantic marine air. Large west African
490 cities such as Dakar and Nouakchott, and/or the shipping lanes to the east/northeast of Cabo
491 Verde, are potential candidates for the source of elevated NO_x. The NO mixing ratios measured
492 in October are higher than those in April and lower than in December. This may be due in part
493 to the influence of polluted African air arriving at Cabo Verde, which is more prominent in



494 October than in April, but less so than in December. The NO_2 and the total NO_x ($\text{NO} + \text{PLC}$
495 NO_2 , figure 9) similarly show higher levels in December than April, but the mixing ratios
496 observed in October are similar to those in April. It should be noted that some of the days with
497 high percentages of African air have missing data or wind directions from other places than the
498 north east.

499 From table 3 it can be observed that the NO , NO_2 , and NO_x measurements at the CVAO
500 compare well to the few other measurements in the remote marine boundary layer as well as
501 background sites in Alert, Canada and measurements in the free troposphere. A wintertime
502 seasonal increase in NO , NO_2 , and NO_x can be observed during December-February, which
503 corresponds to the months when surface air masses arrive at Cabo Verde from western Africa
504 (Carpenter et al., 2010; Lee et al., 2009).

505

506 6 Conclusion

507 A photolytic NO_2 converter with external diodes and a quartz photolysis cell (PLC) has
508 been installed at the Cape Verde Atmospheric Observatory and the NO_2 measurements have
509 been compared to those of the historical BLC used at the site, which has internal diodes and a
510 reaction chamber made of Teflon-like barium doped material. The two measurements show
511 good agreement ($\text{PLC NO}_2 = 0.92 \times \text{BLC NO}_2$, $R^2 = 0.92$) with small differences due to
512 uncertainties in the estimations of the BLC NO_2 artefact. Even though the PLC has a lower
513 conversion efficiency ($\text{CE} = 52 \pm 4\%$) than the BLC ($\text{CE} = 85 \pm 4\%$), it is preferred due to its
514 assumed negligible artefact as a consequence of having non-porous/non-reactive walls. The
515 assumption of a zero artefact causes the hourly uncertainty of the NO_2 measurements to be
516 roughly halved. With 2σ hourly precisions of 0.96 ± 0.89 pptV, 1.45 ± 0.82 pptV, and $2.74 \pm$
517 2.18 pptV and 2σ hourly uncertainties of 1.42 ± 1.47 pptV, 8.38 ± 7.46 pptV, and 4.44 ± 5.79
518 pptV for NO , NO_2 BLC, and NO_2 PLC, respectively, the instrument has a high repeatability
519 and low uncertainties for all the measurements. The mixing ratios observed at the CVAO (NO :
520 2-10 pptV, NO_2 : 5-50 pptV, and NO_x : 7-60 pptV at midday) are in agreement with previous
521 measurements at the CVAO as well as other previous remote measurements around the world.

522



523 7 Data availability

524 The processed data is available through Ebas
525 (<http://ebas.nilu.no/Pages/DataSetList.aspx?key=45DB99FE2B7F4F97864ECF800E71E5D5>
526) and through CEDA (Center for Environmental Data Analysis,
527 <https://catalogue.ceda.ac.uk/uuid/d5422d54d519ed056cc17e97037732b8>).

528

529 8 Author contribution

530 LN runs the instrument on a day-to-day basis. MW and STA wrote the script processing the
531 data. MJR ran the back trajectory analysis. BSN developed the photolytic converter setup. All
532 authors were involved in the analysis, data evaluation and discussion of the results. STA wrote
533 the paper with contributions from all coauthors. All coauthors proofread and commented on
534 the paper.

535

536 9 Competing interests

537 The authors declare that they have no conflict of interest.

538

539 10 Acknowledgements

540 The authors would like to thank Franz Rohrer (Forschungszentrum Jülich) and Tomás Sherwen
541 (University of York) for scientific discussions, and NERC/NCAS for funding the CVAO
542 programme. STA's PhD was funded through the NERC SPHERES Doctoral Training
543 Partnership and the University of York.

544



11 Tables

Table 1: The mean $\pm 2\sigma$ of the standard deviation and difference in counts/s between two subsequent measurement cycles.

Measurement	Standard deviation (%)^a	Difference in counts/s^b	Extreme values (pptV)^c	Extreme difference between mean and median (pptV)^d
Zero	2.4 ± 1.7	-	-	-
NO	2.5 ± 10.6	0 ± 515	1.7 ± 47.9	0.2 ± 4.1
NO ₂ BLC	2.5 ± 7.5	0 ± 1432	16.8 ± 175.2	1.5 ± 33.0
NO ₂ PLC	2.1 ± 2.5	0 ± 738	17.3 ± 176.8	1.7 ± 33.0

^aDetermined as the standard deviation of a cycle divided by the mean. ^bThe difference in counts/s between each cycle. ^cCalculated as the hourly mean ± 4 standard deviations of the hourly mixing ratio. ^dCalculated as the hourly mean ± 4 standard deviations of the differences between the mean and median.



Table 2: Calculated uncertainties associated with the NO_x measurements. The values in bold are the combined uncertainties for each type of measurement. Each uncertainty is given as the mean uncertainty ± 2 standard deviation of the data between January 2014 and August 2019 for NO and from March 2017 to August 2019 for both NO₂ measurements.

Source of uncertainty	Probability distribution	Uncertainty (%)	Uncertainty (pptV)
Hourly precision/repeatability NO	Normal		0.96 ± 0.89
Hourly precision/repeatability NO ₂ BLC	Normal		1.45 ± 0.82
Hourly precision/repeatability NO ₂ PLC	Normal		2.74 ± 2.18
Total Calibration uncertainty NO ^a		2.78 ± 8.05	0.03 ± 0.27
Total Calibration uncertainty NO ₂ BLC ^a		3.44 ± 9.32	0.33 ± 1.27
Total Calibration uncertainty NO ₂ PLC ^a		3.52 ± 8.67	0.37 ± 1.27
Total NO artefact uncertainty ^b			1.05 ± 3.44
Total NO ₂ artefact uncertainty ^b			7.19 ± 7.24
Hourly O ₃ correction uncertainty NO	Normal	20.00 ± 0.001	0.27 ± 1.14
Hourly O ₃ correction uncertainty NO ₂ BLC	Normal	20.00 ± 0.001	2.47 ± 6.75
Hourly O ₃ correction uncertainty NO ₂ PLC	Normal	20.00 ± 0.001	2.60 ± 6.37
Total hourly uncertainty NO			1.42 ± 1.47
Total hourly uncertainty NO ₂ BLC			8.38 ± 7.46
Total hourly uncertainty NO ₂ PLC			4.44 ± 5.79

^aThe individual uncertainties associated with the calibration can be found in table S1. ^bThe individual uncertainties associated with the artefact determination can be found in table S2.



Table 3: NO, NO₂, and NO_x mixing ratios at different low NO_x sites.

	NO (pptV) ^k	NO ₂ (pptV)	NO _x (pptV)	Reference
Tropospheric Marine				
CVAO, Cape Verde 2017-2018	2-10	5-50	7-60	This study
Cape Grim, Australia ^a	1-6	3-6	4-12	(Monks et al., 1998)
SAGA3, Pacific Ocean, Cruise ^b	2.9 ± 0.1			(Torres and Thompson, 1993)
ASTEX, North Atlantic, Cruise ^c	5 ± 4	29 ± 8		(Carsey et al., 1997)
WOCE, Indian Ocean, Cruise ^d	~ 5	18-40		(Rhoads et al., 1997)
Background Sites				
Alert, Canada ^e	0.2-2.8	1.3-10.8		(Beine et al., 2002)
South Pole ^f	~ 10			(Jones et al., 1999)
Free Troposphere				
Mauna Loa, USA ^g	9.4	29.6	32	(Carroll et al., 1992)
Pico Mountain, Portugal ^h	0-9	19-30	20-37	(Val Martin et al., 2008)
NASA GTE, Pacific Ocean, Aircraft ⁱ	~ 1			(Ridley et al., 1987)
Svalbard, Norway ^j			27.7 ± 24.0	(Beine et al., 1996)

^aMeasurements made during the SOAPEX (Southern Ocean Atmospheric Photochemistry EXperiment) campaign during Austral summer in 1995. ^bMeasurements from the Soviet-American Gases and Aerosols (SAGA) campaign between Hawaii and American Samoa between February and March. ^cMeasurements from 6 clean days on the Atlantic Stratocumulus Transition Experiment (ASTEX). ^dMeasurements from the World Ocean Circulation Experiment (WOCE) between South Africa and Sri Lanka. ^eMeasurements made during 24-hour darkness and in spring. ^fMeasurements made from January-March 1997 at the German Antarctic research station, Neumayer. ^gMeasurements made during the Mauna Loa Observatory Photochemistry Experiment (MLOPEX) in May 1988. ^hMeasurements made at Mount Pico between July 2002 and August 2005. ⁱMeasurements made in the upper marine boundary layer from 13 flights between California and west of Hawaii. ^jMeasurements made at the Ny-Ålesund Zeppelin mountain station on Svalbard during a spring campaign in 1994. ^kDaytime values.



12 Figures

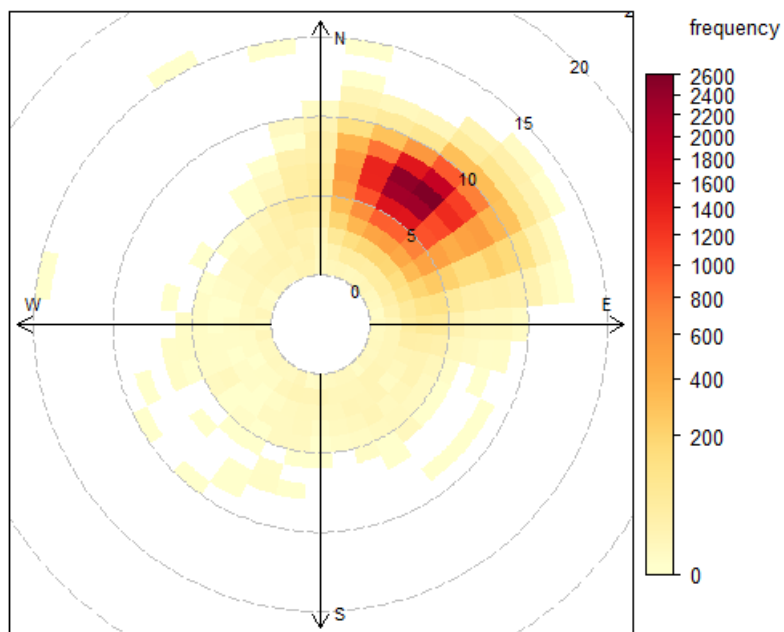


Figure 1: The frequency of hourly averaged wind speed and direction from January 2014 to August 2019. Each square symbolise 10 degrees of wind direction and 1 m/s wind speed. Each dashed circle show an increase in wind speed of 5 m/s.

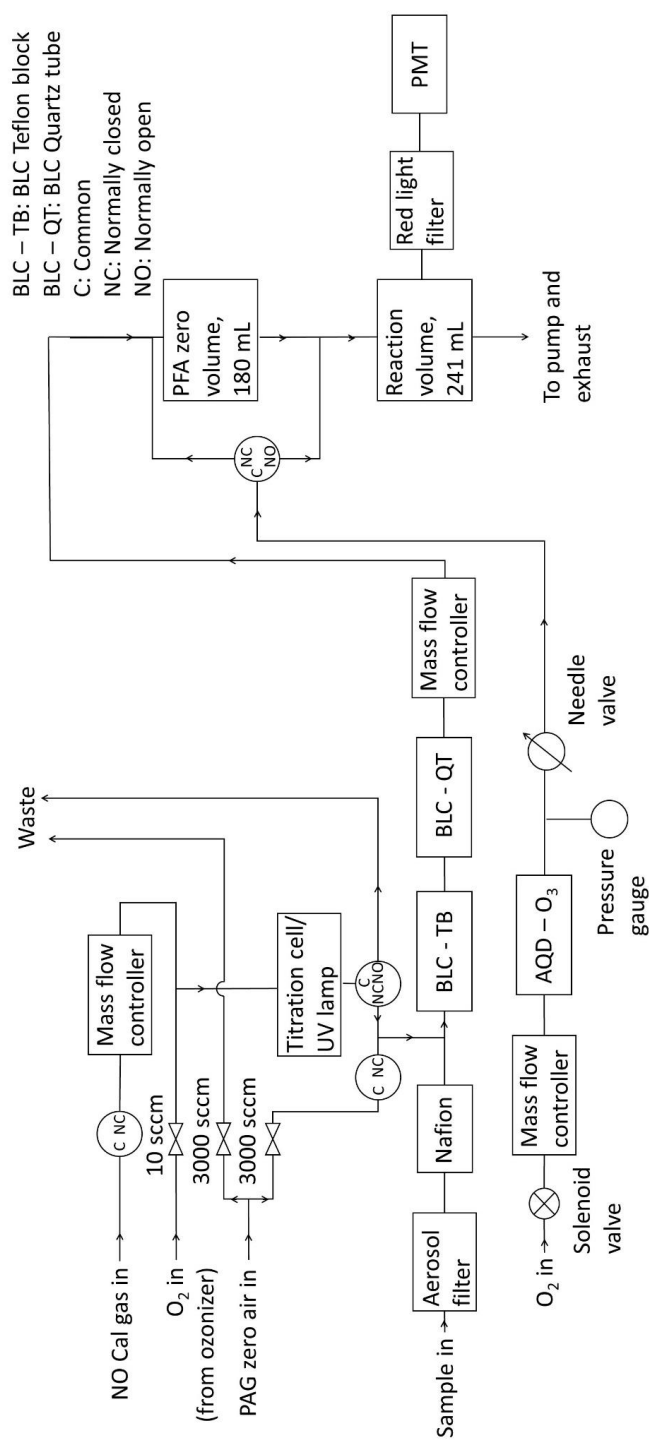


Figure 2: Flow diagram of the NO_x instrument at the CVAO.

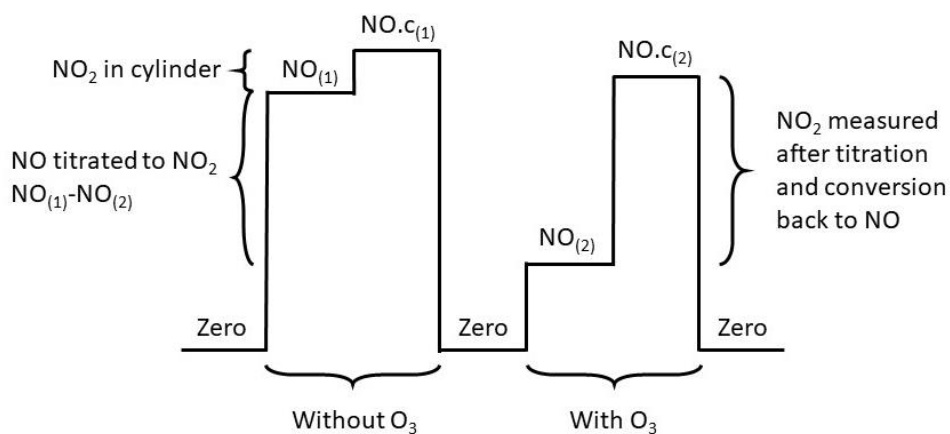


Figure 3: A theoretical calibration cycle. “NO” is the measurement of only NO i.e. when the converters are off, NO.c is when one of the converters are on therefore the measurement is NO + NO₂ and (1) and (2) represent untitrated and titrated NO, respectively.

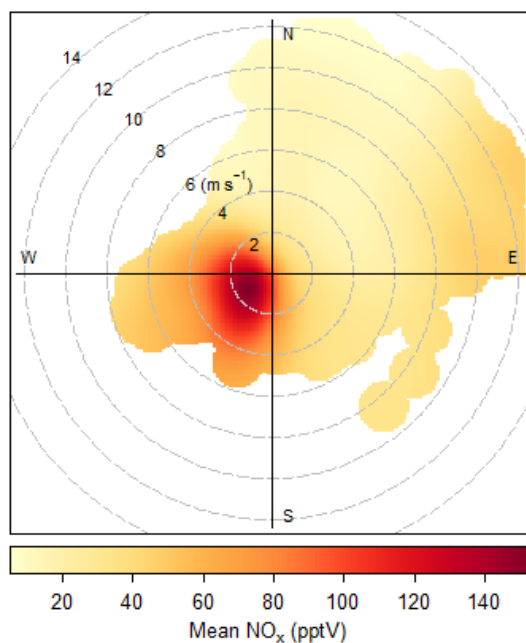


Figure 4: Total NO_x from June 2017 to August 2019 plotted as a function of wind speed and direction.

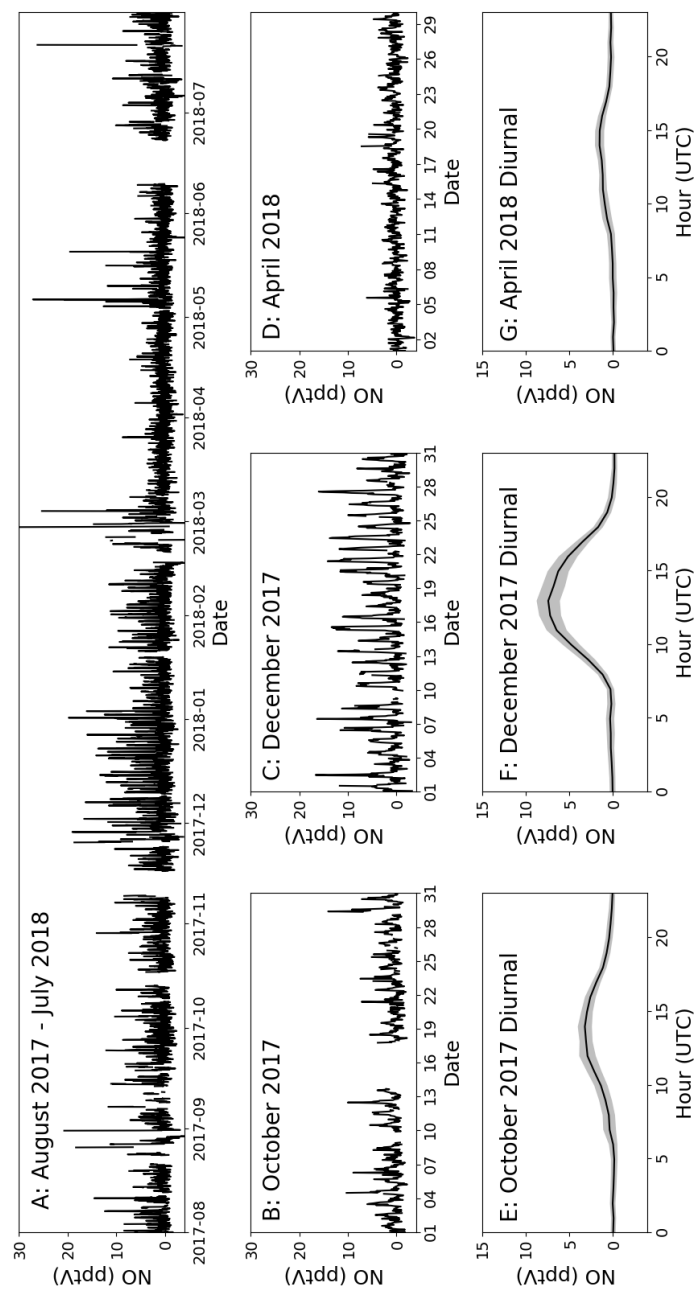


Figure 5: Panel A show the time series for filtered O₃ corrected NO from August 1st 2017 to July 31st 2018. Panel B, C and D zoom in on October 2017, December 2017 and April 2018, respectively. Panel E, F and G show the average diurnal of NO for October 2017, December 2017 and April 2018, respectively, with the coloured areas being ± 2 standard errors. If there are less than 15 measurements available for the hour, it is not included in the diurnal.

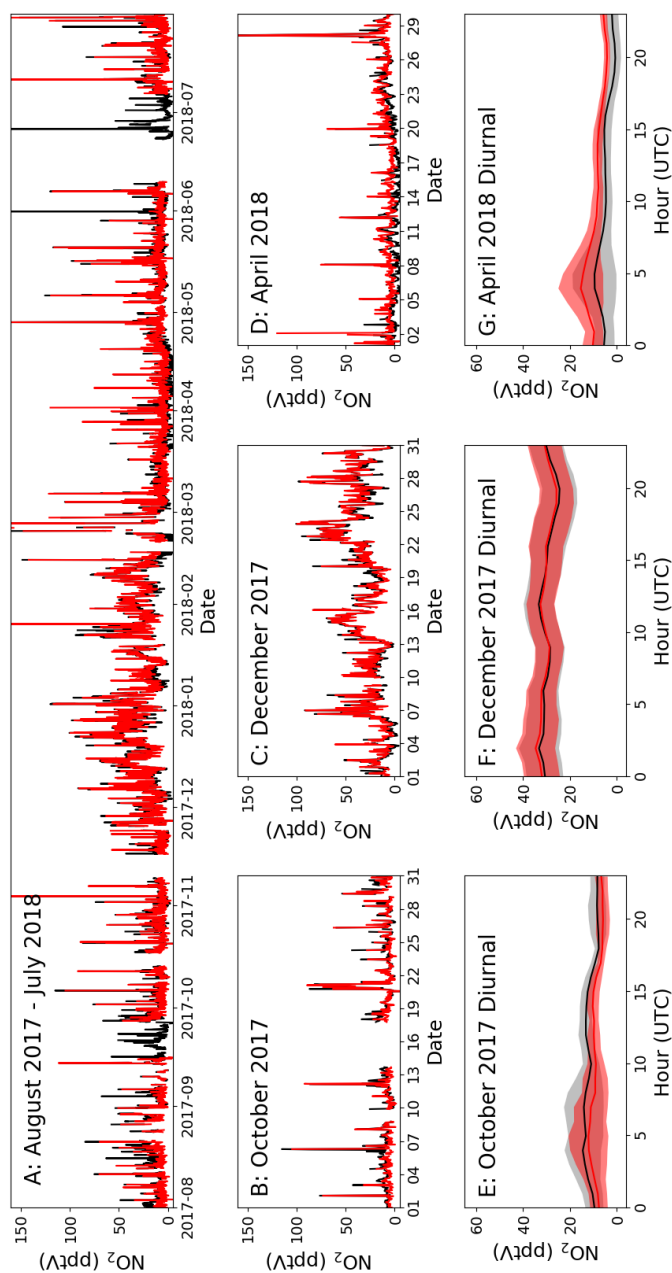


Figure 6: Panel A show the time series of filtered O_3 corrected NO_2 from August 1st 2017 to July 31st 2018 for the BLC (black) and PLC (red). Panel B, C and D zoom in on October 2017, December 2017 and April 2018, respectively, with the red line being the PLC and the black being the BLC. Panel E, F and G show the average diurnal of NO_2 for October 2017, December 2017 and April 2018, respectively, with the red line being the PLC and the black being the BLC and the coloured areas being ± 2 standard errors. If there are less than 15 measurements available for the hour, it is not included in the diurnal.

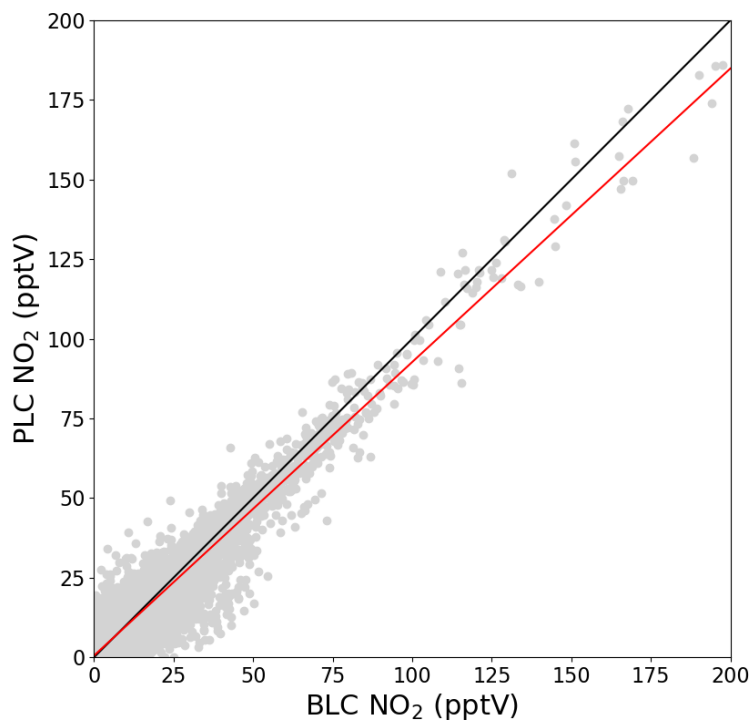


Figure 7: The PLC NO₂ concentration is plotted against the BLC NO₂ concentration. The black lines show the 1-to-1 relationship. The red line is the linear regression of the hourly data with uncertainties in both the x and y.

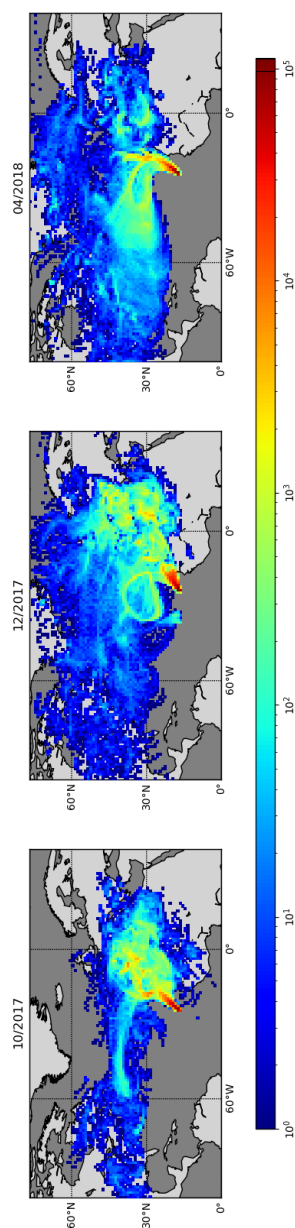


Figure 8: Back trajectories estimated for October 2017, December 2017, and April 2018. FLEXPART version 10.4 is used in backwards mode, driven by pressure level data from Global Forecast System (GFS) reanalyses at $0.5^\circ \times 0.5^\circ$ resolution (Pisso et al., 2019; Stohl et al., 1998). 10-day back-trajectory simulations are initialised every 6 hours, releasing 1000 particles from the CVAO site.

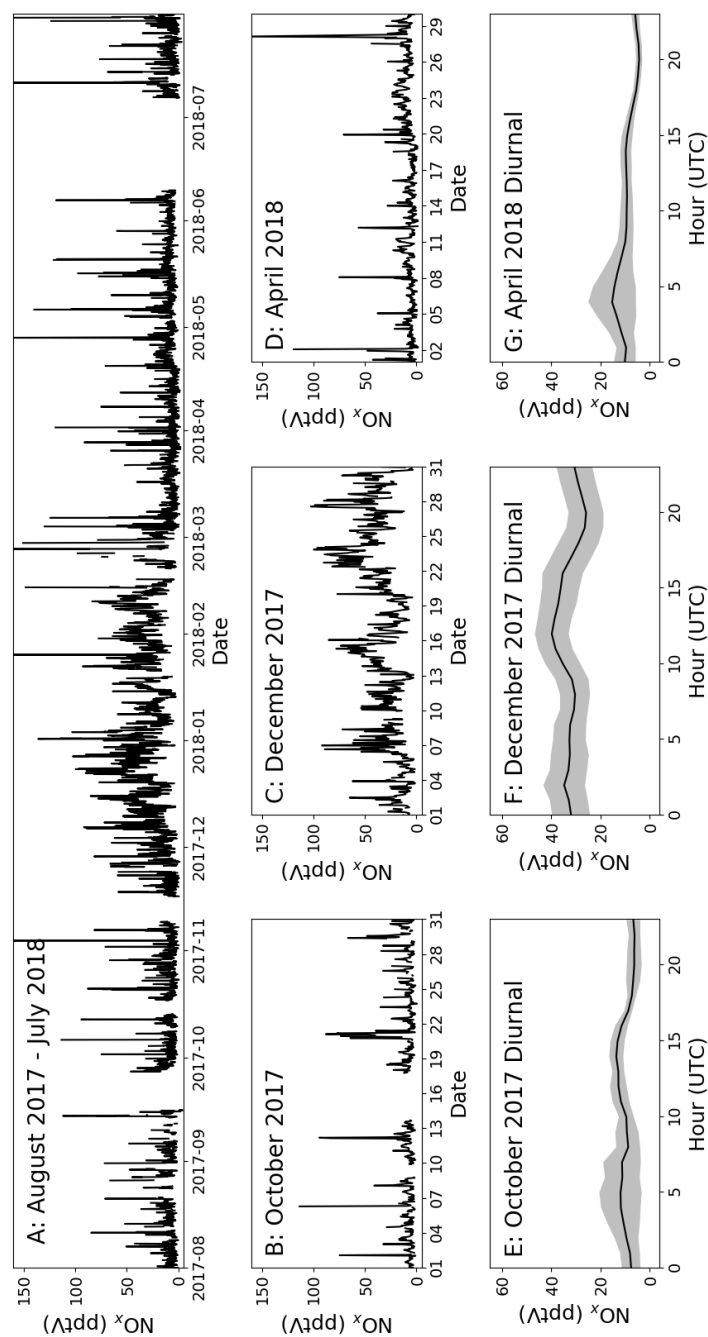


Figure 9: Panel A show the time series for total NO_x (NO + NO₂ PLC) from August 1st 2017 to July 31st 2018. Panel B, C and D zoom in on October 2017, December 2017 and April 2018, respectively. Panel E, F and G show the average diurnal of NO_x for October 2017, December 2017 and April 2018, respectively, with the coloured areas being ±2 standard errors. If there are less than 15 measurements available for the hour, it is not included in the diurnal.



References

- Alam, M. S., Crilley, L. R., Lee, J. D., Kramer, L. J., Pfrang, C., Vázquez-Moreno, M., Muñoz, A., Ródenas, M., and Bloss, W. J.: Interference from alkenes in chemiluminescent NO_x measurements, *Atmos. Meas. Tech. Discuss.*, 2020, 1-26, [10.5194/amt-2020-164](https://doi.org/10.5194/amt-2020-164), 2020.
- Atkinson, R.: Atmospheric chemistry of VOCs and NO_x, *Atmospheric Environment*, 34, 2063-2101, [https://doi.org/10.1016/S1352-2310\(99\)00460-4](https://doi.org/10.1016/S1352-2310(99)00460-4), 2000.
- Atkinson, R., Baulch, D. L., Cox, R. A., Crowley, J. N., Hampson, R. F., Hynes, R. G., Jenkin, M. E., Rossi, M. J., and Troe, J.: Evaluated kinetic and photochemical data for atmospheric chemistry: Volume I - gas phase reactions of Ox, HO_x, NO_x and SO_x species, *Atmos. Chem. Phys.*, 4, 1461-1738, [10.5194/acp-4-1461-2004](https://doi.org/10.5194/acp-4-1461-2004), 2004.
- Beine, H. J., Engardt, M., Jaffe, D. A., Hov, Ø., Holme'n, K., and Stordal, F.: Measurements of NO_x and aerosol particles at the NY-A'lesund Zeppelin mountain station on Svalbard: Influence of regional and local pollution sources, *Atmospheric Environment*, 30, 1067-1079, [https://doi.org/10.1016/1352-2310\(95\)00410-6](https://doi.org/10.1016/1352-2310(95)00410-6), 1996.
- Beine, H. J., Honrath, R. E., Dominé, F., Simpson, W. R., and Fuentes, J. D.: NO_x during background and ozone depletion periods at Alert: Fluxes above the snow surface, *Journal of Geophysical Research: Atmospheres*, 107, ACH 7-1-ACH 7-12, [10.1029/2002jd002082](https://doi.org/10.1029/2002jd002082), 2002.
- Bell, S.: *A Beginner's Guide to Uncertainty of Measurement*, NPL, 1999.
- Buhr, M. P.: Solid-state light source photolytic nitrogen dioxide converter, in, edited by: USPTO, USA, 2007.
- Carpenter, L. J., Fleming, Z. L., Read, K. A., Lee, J. D., Moller, S. J., Hopkins, J. R., Purvis, R. M., Lewis, A. C., Müller, K., Heinold, B., Herrmann, H., Fomba, K. W., van Pinxteren, D., Müller, C., Tegen, I., Wiedensohler, A., Müller, T., Niedermeier, N., Achterberg, E. P., Patey, M. D., Kozlova, E. A., Heimann, M., Heard, D. E., Plane, J. M. C., Mahajan, A., Oetjen, H., Ingham, T., Stone, D., Whalley, L. K., Evans, M. J., Pilling, M. J., Leigh, R. J., Monks, P. S., Karunaharan, A., Vaughan, S., Arnold, S. R., Tschritter, J., Pöhler, D., Frieß, U., Holla, R., Mendes, L. M., Lopez, H., Faria, B., Manning, A. J., and Wallace, D. W. R. J. J. o. A. C.: Seasonal characteristics of tropical marine boundary layer air measured at the Cape Verde Atmospheric Observatory, 67, 87-140, [10.1007/s10874-011-9206-1](https://doi.org/10.1007/s10874-011-9206-1), 2010.
- Carroll, M. A., Ridley, B. A., Montzka, D. D., Hubler, G., Walega, J. G., Norton, R. B., Huebert, B. J., and Grahek, F. E.: Measurements of nitric oxide and nitrogen dioxide during the Mauna Loa Observatory Photochemistry Experiment, *Journal of Geophysical Research: Atmospheres*, 97, 10361-10374, [10.1029/91jd02296](https://doi.org/10.1029/91jd02296), 1992.
- Carsey, T. P., Churchill, D. D., Farmer, M. L., Fischer, C. J., Pszenny, A. A., Ross, V. B., Saltzman, E. S., Springer-Young, M., and Bonsang, B.: Nitrogen oxides and ozone production in the North Atlantic marine boundary layer, *Journal of Geophysical Research: Atmospheres*, 102, 10653-10665, [10.1029/96JD03511](https://doi.org/10.1029/96JD03511), 1997.
- Carslaw, D. C.: Evidence of an increasing NO₂/NO_x emissions ratio from road traffic emissions, *Atmospheric Environment*, 39, 4793-4802, <https://doi.org/10.1016/j.atmosenv.2005.06.023>, 2005.
- Chiapello, I., Bergametti, G., Gomes, L., Chatenet, B., Dulac, F., Pimenta, J., and Soares, E. S.: An additional low layer transport of Sahelian and Saharan dust over the north-eastern Tropical Atlantic, *Geophysical Research Letters*, 22, 3191-3194, [10.1029/95gl03313](https://doi.org/10.1029/95gl03313), 1995.
- Clough, P., and Thrush, B. A.: Mechanism of chemiluminescent reaction between nitric oxide and ozone, *Transactions of the Faraday Society*, 63, 915-925, 1967.
- Clyne, M. A. A., Thrush, B. A., and Wayne, R. P.: Kinetics of the chemiluminescent reaction between nitric oxide and ozone, *Transactions of the Faraday Society*, 60, 359-370, [10.1039/TF9646000359](https://doi.org/10.1039/TF9646000359), 1964.
- Drummond, J. W., Volz, A., and Ehhalt, D. H. J. J. o. a. c.: An optimized chemiluminescence detector for tropospheric NO measurements, 2, 287-306, 1985.



- Dunlea, E. J., Herndon, S. C., Nelson, D. D., Volkamer, R. M., San Martini, F., Sheehy, P. M., Zahniser, M. S., Shorter, J. H., Wormhoudt, J. C., Lamb, B. K., Allwine, E. J., Gaffney, J. S., Marley, N. A., Grutter, M., Marquez, C., Blanco, S., Cardenas, B., Retama, A., Ramos Villegas, C. R., Kolb, C. E., Molina, L. T., and Molina, M. J.: Evaluation of nitrogen dioxide chemiluminescence monitors in a polluted urban environment, *Atmos. Chem. Phys.*, 7, 2691-2704, 10.5194/acp-7-2691-2007, 2007.
- Finlayson, B. J., Pitts, J. N., and Atkinson, R.: Low-pressure gas-phase ozone-olefin reactions. Chemiluminescence, kinetics, and mechanisms, *Journal of the American Chemical Society*, 96, 5356-5367, 10.1021/ja00824a009, 1974.
- Fomba, K. W., Müller, K., van Pinxteren, D., Poulain, L., van Pinxteren, M., and Herrmann, H.: Long-term chemical characterization of tropical and marine aerosols at the Cape Verde Atmospheric Observatory (CVAO) from 2007 to 2011, *Atmos. Chem. Phys.*, 14, 8883-8904, 10.5194/acp-14-8883-2014, 2014.
- Fontijn, A., Sabadell, A. J., and Ronco, R. J.: Homogeneous chemiluminescent measurement of nitric oxide with ozone. Implications for continuous selective monitoring of gaseous air pollutants, *Analytical chemistry*, 42, 575-579, 1970.
- Galbally, I. E.: Nitrogen Oxides (NO, NO₂, NO_y) measurements at Cape Grim: A technical manual Baseline Atmospheric Program Australia, Technical Series, 111, 2019.
- Gilge, S., Plass-Dülmer, C., Rohrer, F., Steinbacher, M., Fjaeraa, A. M., Lagler, F., and Walden, J.: WP4-NA4: Trace gases networking: Volatile organic carbon and nitrogen oxides Deliverable D4.10: Standardized operating procedures (SOPs) for NO_x measurements, ACTRIS, 2014.
- Grosjean, D., and Harrison, J.: Response of chemiluminescence NO_x analyzers and ultraviolet ozone analyzers to organic air pollutants, *Environmental Science & Technology*, 19, 862-865, 10.1021/es00139a016, 1985.
- Jaeglé, L., Jacob, D. J., Brune, W. H., Tan, D., Faloon, I. C., Weinheimer, A. J., Ridley, B. A., Campos, T. L., and Sachse, G. W.: Sources of HO_x and production of ozone in the upper troposphere over the United States, *Geophysical Research Letters*, 25, 1709-1712, 10.1029/98gl00041, 1998.
- Jones, A. E., Weller, R., Minikin, A., Wolff, E. W., Sturges, W. T., McIntyre, H. P., Leonard, S. R., Schrems, O., and Bauguitte, S.: Oxidized nitrogen chemistry and speciation in the Antarctic troposphere, *Journal of Geophysical Research: Atmospheres*, 104, 21355-21366, 10.1029/1999jd900362, 1999.
- Kley, D., and McFarland, M.: Chemiluminescence detector for NO and NO₂, *Atmos. Technol. (United States)*, 12, 1980.
- Lee, J. D., Moller, S. J., Read, K. A., Lewis, A. C., Mendes, L., and Carpenter, L. J.: Year-round measurements of nitrogen oxides and ozone in the tropical North Atlantic marine boundary layer, *Journal of Geophysical Research: Atmospheres*, 114, 2009.
- Logan, J. A.: Tropospheric ozone: Seasonal behavior, trends, and anthropogenic influence, 90, 10463-10482, doi:10.1029/JD090iD06p10463, 1985.
- Matthews, R. D., Sawyer, R. F., and Schefer, R. W.: Interferences in chemiluminescent measurement of nitric oxide and nitrogen dioxide emissions from combustion systems, *Environmental Science & Technology*, 11, 1092-1096, 10.1021/es60135a005, 1977.
- Mazzeo, N. A., Venegas, L. E., and Choren, H.: Analysis of NO, NO₂, O₃ and NO_x concentrations measured at a green area of Buenos Aires City during wintertime, *Atmospheric Environment*, 39, 3055-3068, <https://doi.org/10.1016/j.atmosenv.2005.01.029>, 2005.
- Monks, P. S., Carpenter, L. J., Penkett, S. A., Ayers, G. P., Gillett, R. W., Galbally, I. E., and Meyer, C. P.: Fundamental ozone photochemistry in the remote marine boundary layer: the soapex experiment, measurement and theory, *Atmospheric Environment*, 32, 3647-3664, [https://doi.org/10.1016/S1352-2310\(98\)00084-3](https://doi.org/10.1016/S1352-2310(98)00084-3), 1998.
- Pandey, S. K., Kim, K.-H., Chung, S.-Y., Cho, S. J., Kim, M. Y., and Shon, Z.-H.: Long-term study of NO_x behavior at urban roadside and background locations in Seoul, Korea, *Atmospheric Environment*, 42, 607-622, <https://doi.org/10.1016/j.atmosenv.2007.10.015>, 2008.



- Peterson, M. C., and Honrath, R. E.: NO_x and NO_y over the northwestern North Atlantic: Measurements and measurement accuracy, *Journal of Geophysical Research: Atmospheres*, 104, 11695-11707, 1999.
- Pisso, I., Sollum, E., Grythe, H., Kristiansen, N. I., Cassiani, M., Eckhardt, S., Arnold, D., Morton, D., Thompson, R. L., Groot Zwaafink, C. D., Evangelidou, N., Sodemann, H., Haimberger, L., Henne, S., Brunner, D., Burkhardt, J. F., Fouilloux, A., Brioude, J., Philipp, A., Seibert, P., and Stohl, A.: The Lagrangian particle dispersion model FLEXPART version 10.4, *Geosci. Model Dev.*, 12, 4955-4997, 10.5194/gmd-12-4955-2019, 2019.
- Pollack, I. B., Lerner, B. M., and Ryerson, T. B.: Evaluation of ultraviolet light-emitting diodes for detection of atmospheric NO₂ by photolysis - chemiluminescence, *Journal of Atmospheric Chemistry*, 65, 111-125, 10.1007/s10874-011-9184-3, 2010.
- Read, K. A., Mahajan, A. S., Carpenter, L. J., Evans, M. J., Faria, B. V. E., Heard, D. E., Hopkins, J. R., Lee, J. D., Moller, S. J., Lewis, A. C., Mendes, L., McQuaid, J. B., Oetjen, H., Saiz-Lopez, A., Pilling, M. J., and Plane, J. M. C.: Extensive halogen-mediated ozone destruction over the tropical Atlantic Ocean, *Nature*, 453, 1232, 10.1038/nature07035
- <https://www.nature.com/articles/nature07035#supplementary-information>, 2008.
- Reed, C., Evans, M. J., Carlo, P. D., Lee, J. D., Carpenter, L. J. J. A. C., and Physics: Interferences in photolytic NO₂ measurements: explanation for an apparent missing oxidant?, 16, 4707-4724, 2016.
- Reed, C., Evans, M. J., Crilley, L. R., Bloss, W. J., Sherwen, T., Read, K. A., Lee, J. D., and Carpenter, L. J.: Evidence for renoxification in the tropical marine boundary layer, *Atmos. Chem. Phys.*, 17, 4081-4092, 10.5194/acp-17-4081-2017, 2017.
- Rhoads, K. P., Kelley, P., Dickerson, R. R., Carsey, T. P., Farmer, M., Savoie, D. L., and Prospero, J. M.: Composition of the troposphere over the Indian Ocean during the monsoonal transition, *Journal of Geophysical Research: Atmospheres*, 102, 18981-18995, 10.1029/97JD01078, 1997.
- Ridley, B. A., Carroll, M. A., and Gregory, G. L.: Measurements of nitric oxide in the boundary layer and free troposphere over the Pacific Ocean, *Journal of Geophysical Research: Atmospheres*, 92, 2025-2047, 10.1029/JD092iD02p02025, 1987.
- Ridley, B. A., and Grahek, F. E.: A Small, Low Flow, High Sensitivity Reaction Vessel for NO Chemiluminescence Detectors, *Journal of Atmospheric and Oceanic Technology*, 7, 307-311, 10.1175/1520-0426(1990)007<0307:Aslfs>2.0.Co;2, 1990.
- Ridley, B. A., Grahek, F. E., and Walega, J. G.: A Small High-Sensitivity, Medium-Response Ozone Detector Suitable for Measurements from Light Aircraft, *Journal of Atmospheric and Oceanic Technology*, 9, 142-148, 10.1175/1520-0426(1992)009<0142:Ashsmr>2.0.Co;2, 1992.
- Rijkenberg, M. J. A., Powell, C. F., Dall'Osto, M., Nielsdottir, M. C., Patey, M. D., Hill, P. G., Baker, A. R., Jickells, T. D., Harrison, R. M., and Achterberg, E. P.: Changes in iron speciation following a Saharan dust event in the tropical North Atlantic Ocean, *Marine Chemistry*, 110, 56-67, <https://doi.org/10.1016/j.marchem.2008.02.006>, 2008.
- Ryall, D. B., Derwent, R. G., Manning, A. J., Simmonds, P., and O'Doherty, S.: Estimating source regions of European emissions of trace gases from observations at Mace Head, 2507-2523 pp., 2001.
- Ryerson, T. B., Williams, E. J., and Fehsenfeld, F. C.: An efficient photolysis system for fast-response NO₂ measurements, *Journal of Geophysical Research: Atmospheres*, 105, 26447-26461, 10.1029/2000jd900389, 2000.
- Stohl, A., Hittenberger, M., and Wotawa, G.: Validation of the lagrangian particle dispersion model FLEXPART against large-scale tracer experiment data, *Atmospheric Environment*, 32, 4245-4264, [https://doi.org/10.1016/S1352-2310\(98\)00184-8](https://doi.org/10.1016/S1352-2310(98)00184-8), 1998.
- Torres, A. L., and Thompson, A. M.: Nitric oxide in the equatorial Pacific boundary layer: SAGA 3 measurements, *Journal of Geophysical Research: Atmospheres*, 98, 16949-16954, 10.1029/92jd01906, 1993.



- Val Martin, M., Honrath, R., Owen, R. C., Pfister, G., Fialho, P., and Barata, F. J. J. o. G. R. A.: Significant enhancements of nitrogen oxides, black carbon, and ozone in the North Atlantic lower free troposphere resulting from North American boreal wildfires, 111, 2006.
- Val Martin, M., Honrath, R. E., Owen, R. C., and Li, Q. B.: Seasonal variation of nitrogen oxides in the central North Atlantic lower free troposphere, *Journal of Geophysical Research: Atmospheres*, 113, 10.1029/2007jd009688, 2008.
- Winer, A. M., Peters, J. W., Smith, J. P., and Pitts, J. N.: Response of commercial chemiluminescent nitric oxide-nitrogen dioxide analyzers to other nitrogen-containing compounds, *Environmental Science & Technology*, 8, 1118-1121, 10.1021/es60098a004, 1974.